Friction stir welding of pure titanium lap joint

H. Liu*[1], K. Nakata[1], N. Yamamoto[2] and J. Liao[2]

The effects of welding parameters on friction stir welding of pure titanium lap joint were investigated together with the microstructural characteristics of the sound joint. Three kinds of welding defects were found under the condition of tool load control, namely, the groove-like defect, the inner cavity defect and the overheating rough surface and tool penetration defect with increasing heat input. The tool plunge depth control effectively increased the lap width compared with the tool load control, so the sound joints fractured in the base metal were acquired at 250 rev min^{-1}–75 mm min^{-1} and 200 rev min^{-1}–50 mm min^{-1}. The sound joint consisted of the thermomechanically affected zone, the stir zone, the lap zone and the top layer. The microstructure was fined obviously after welding, and finer grains were observed in the lap zone and top layer.

Keywords: Friction stir welding, Pure titanium, Lap joint, Welding defect, Shear strength, Microstructural characteristics

Introduction

Friction stir welding (FSW) is an innovative solid state welding process invented in 1991 by Thomas *et al.*[1] Since the appearance of FSW, it has gained considerable interests due to the avoidance of solidification problems associated with conventional fusion welding techniques,[2–4] and has been successfully applied to the low melting metals such as Al alloys and Mg alloys.[5–11] In recent years, a great deal of attention has been focused on the FSW of high melting metals with the continued development of FSW technique,[12–16] especially for titanium and its alloys because of the wide application in the industrial field.[17–26] However, it should be pointed out that it is extraordinarily arduous to friction stir weld the titanium and its alloys owing to the high activity, high melting point and low heat diffusivity. Fortunately, a large number of researches have been performed, including the microstructural characteristics,[17–19,21] the mechanical properties,[20,25,26] the material flow and the grain structure evolution.[22–24] The published papers have mainly concentrated on the butt joint of titanium and its alloys, but little work has reported the FSW of lap joint. In the present study, the FSW of pure titanium lap joint was carried out, the effects of welding parameters on FSW were investigated extensively and the microstructural characteristics of the sound joint were studied in detail.

Experimental

The material used in this research was a pure titanium sheet with dimensions of $300\times100\times2$ mm, and it had a chemical composition of Ti–0·01C–0·03Fe–0·01N–0·1O–0·001H (wt-%). The FSW of lap joint was carried out under the conditions of tool load or plunge depth control using the WC–Co tool (tilted at 3° from the vertical) with 2·0 mm probe length, which consisted of a 15 mm shoulder and a 6 mm probe in diameter. The axial force was 14·7 kN under the tool load control. The tool plunge depth control was realised by changing the axial force during FSW, which means that the axial force was reduced (or enhanced) automatically with increasing (or decreasing) plunge depth. So the tool was held at the same position approximately and the plunge depth was $\sim$2·3 mm according to the measurement of the macrostructures. The rotational speeds ranging from 200 to 350 rev min^{-1} and welding speeds from 50 to 150 mm min^{-1} were used in this investigation. The water cooling and argon shielding systems were utilised during FSW to cool the tool and minimise surface oxidation.

The joints were cross-sectioned for the metallographic analysis and the lap shear strength was tested by a wire electrical discharge cutting machine (HSC-300; Brother Ind. Ltd, Nagoya, Japan). The cross-sections were mechanically polished using water abrasive paper followed by the 1 μm diamond paste as a final polishing, and then were etched in a solution comprising of hydrofluoric acid, nitric acid and distilled water at a volume ratio of 1 : 1 : 8. Finally, the specimens were observed by an optical microscope (VH-Z100R; Keyence Corp., Osaka, Japan) and a scanning electron microscope (VE-8800; Keyence Corp., Osaka, Japan). The lap shear strength test was evaluated by means of a tensile test machine (Instron-5500R; Instron Corp., Norwood, MA, USA) at room temperature with a crosshead speed of 1 mm min^{-1}. The relative position of pure titanium lap joint for lap shear strength test is shown in Fig. 1. The AS and RS are the advancing side and retreating side respectively. The electron back scattered diffraction was applied to confirm the grain size by the scanning electron microscope (JSM-6400; JEOL Ltd, Tokyo, Japan) incorporated

[1]Joining and Welding Research Institute, Osaka University, Ibaraki 567-0047, Osaka, Japan
[2]Technology Development Headquarters, Kurimoto Ltd, Osaka 559-0021, Japan

*Correspondence author, email liuhong@jwri.osaka-u.ac.jp

Published by Maney on behalf of the Institute
Received 4 May 2010; accepted 29 May 2010
DOI 10.1179/136217110X12731414740031

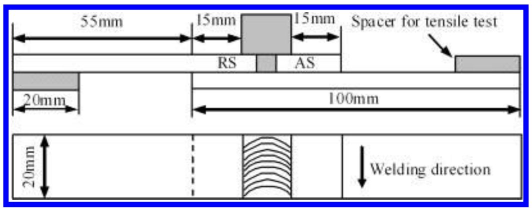

1 Relative position of pure titanium lap joint for lap shear strength test

with TSL (TexSEM Laboratories) (MSC-2200; TexSEM Laboratories Inc., UT, USA). The sample was electropolished at room temperature for 30 s under a potential of 25 V in a solution containing perchloric acid, n-butyl alcohol and methanol at a volume ratio of 1 : 7 : 10.

Results and discussion

Welding defect and shear strength under condition of tool load control

The relationship between the welding parameters and the welding defects under the tool load control is presented in Fig. 2. It can be seen that the groove-like defect was found when welded at high welding speed (or low rotational speed) due to the insufficient heat input. With decreasing welding speed at the same rotational speed (or increasing rotational speed at the same welding speed), the groove-like defect disappeared and the inner cavity defect appeared gradually. Under the appropriate heat input, the joint without defect was obtained at a rotational speed of 250 rev min^{-1} and a welding speed of 75 mm min^{-1}. With a further decrease in welding speed (or increase in rotational speed), the overheating rough surface and tool penetration defect formed because of the excessive heat input. The surface appearances and cross-sections of the defects are shown in Table 1. The groove-like defect was detected in the RS of stir zone (SZ) and the inner cavity defect was observed in the centre part of SZ as the low heat input was adopted. The overheating rough surface and tool penetration defect was shown when the high heat input was employed, which is probably attributed to that the temperature of stirred metal sharply ascended and the $\alpha \rightarrow \beta$ phase transformation happened. A great deal of soft β phase formed in the SZ at high temperature, so

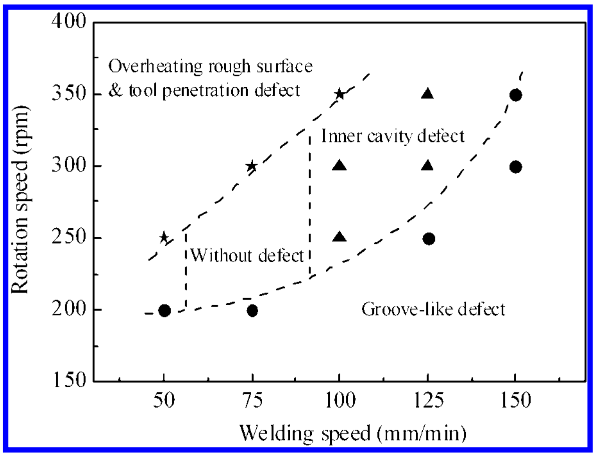

2 Relationship between welding parameters and welding defects under tool load control

the tool rapidly penetrated the bottom titanium plate under the tool load control. At the same time, the titanium metal was extruded from the SZ and much burr occurred in the RS. It can be also seen from Table 1 that the average rotational speed/welding speed parameter (N/V) was calculated to roughly correlate the nature of the defects with the welding heat input.[5] According to the parameter, it has been demonstrated that the groove-like defect gradually changed to the inner cavity defect and the overheating rough surface and tool penetration defect with increasing heat input. However, the groove-like defect close to the start position of weld was found at 200 rev min^{-1}–50 mm min^{-1} and the defect type did not conform to the average N/V parameter. The reason is probably due to the insufficient heat input produced from the low rotational speed during the plunge stage.

The welding parameter, macrostructure, lap width and failure load of the joint without defect under the tool load control are shown in Table 2. It can be found from the macrostructure that the lap interface between the upper and bottom plates partly vanished after FSW. So the lap width was approximately attained by measuring the length of disappeared interface. The lap width was ~2·7 mm and the failure load was ~11·9 kN. More detailed information about the tensile curve of the joint is shown in Fig. 3*a*. The tensile curve quickly increased at the beginning followed by a rapid decrease in the end, and small

Table 1 Surface appearances and cross-sections of welding defects under tool load control

Heat input	Average N/V, mm^{-1}	Welding defect	Surface appearance	Cross-section
Insufficient	2·2	Groove-like defect	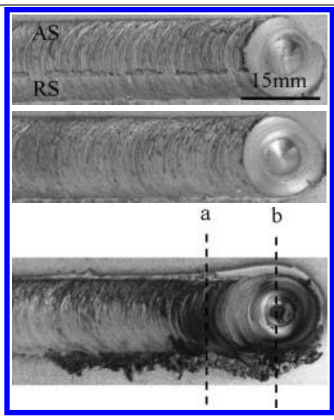	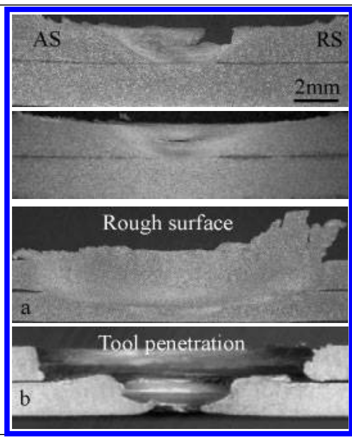
	2·7	Inner cavity defect		
Excessive	4·2	Overheating rough surface and tool penetration defect		

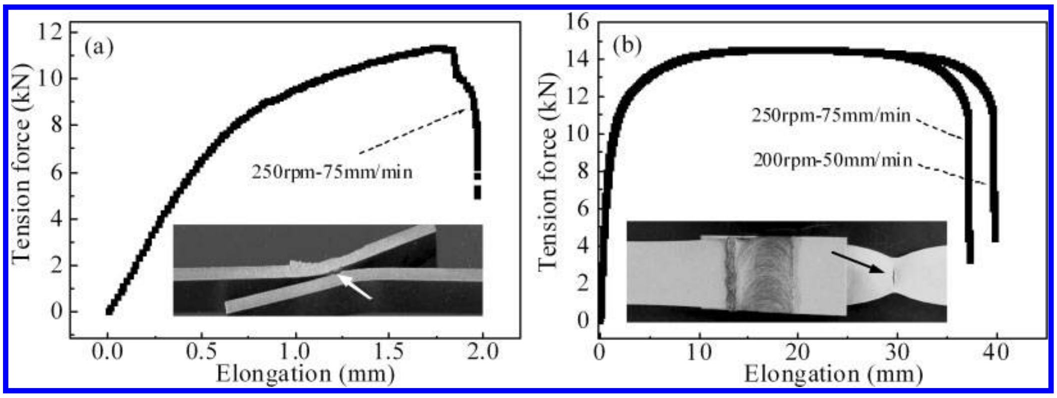

a load control; *b* plunge depth control

3 Tensile curves of joints without defect under conditions of tool

elongation was found in the curve. The short lap width reflected on the weak bonding during FSW, so the fracture happened in the lap zone as shown in the bottom part of Fig. 3*a*.

Obtainment of sound joints under condition of tool plunge depth control

Based on the experiments of tool load control, it can be concluded that the lap width strongly influenced the failure load and the failure load was possibly improved by increasing the lap width. The lap zone can be widened by enhancing the axial force, but the large axial force easily causes the overheating rough surface and tool penetration defect under the tool load control. The FSW was subsequently carried out under the condition of tool plunge depth control and a small range of welding parameters were accomplished in the experiments, which was mainly aimed to obtain the sufficient lap width. The joints without defect were acquired at 250 rev min^{-1}–75 mm min^{-1} and 200 rev min^{-1}–50 mm min^{-1}, the lap widths were up to $\sim$4·5 mm and the failure loads were $\sim$14·5 kN as shown in Table 2. Compared with the joint at 250 rev min^{-1}–75 mm min^{-1} under the tool load control, the lap width obviously increased when welded at the same welding parameter under the tool plunge depth control. The tensile curves of the joints without defect are shown in Fig. 3*b*, and the picture of fracture sample is inserted in the bottom part. The tensile curves quickly ascended at the beginning of the tensile test (elongation$<$10 mm), the curves approximately experienced to be horizontal in the middle (10 mm$\leqslant$elongation$\leqslant$30 mm) and then they sharply descended in the end (elongation$>$30 mm). The enough lap width supplied the sufficient bonding strength in the lap zone, which led to the fracture happening in the base metal (BM) after a large elongation.

Microstructural characteristics of sound joint

The microstructures of the sound joint welded at 250 rev min^{-1}–75 mm min^{-1} under the tool plunge depth control are shown in Fig. 4, and a low magnification overview is displayed in the top part. It can be seen from the overview that the joint was composed of the thermomechanically affected zone (TMAZ), the SZ, the lap zone and the top layer. The lap zone bonding the upper and bottom plate was detected in the bottom part of SZ (SZ-Bottom) and the top layer with a thickness of 0·2 mm was observed in the top part of SZ (SZ-Top). It should be declared that the lap zone and top layer belonged to the SZ. After welding, the microstructures of the TMAZ and SZ were obviously different from those of BM. The grain structure with definite deformation direction was found in the TMAZ. The SZ, experiencing the high temperature and large plastic deformation, was depicted as the fine equiaxed grain structure. The fine grains formed in the SZ result in the increase in the microhardness evidently, and more details about the relationship between the microhardness and grain refinement have been discussed by Fujii *et al.*[27] Figure 5 shows the electron back scattered diffraction maps of different observed regions denoted in Fig. 4. The BM consisted of the equiaxed α phase grains with an average size of 22 μm as seen from Fig. 5*a*. The fine grains with an average size of 8·0 μm were observed in the centre part of SZ (SZ-Centre) as shown in Fig. 5*b*. The lap zone showed the finer grains

Table 2 Welding parameters, macrostructures, lap widths and failure loads of joints without defect under conditions of tool load or plunge depth control

Control system	Rotational speed, rev min^{-1}	Welding speed, mm min^{-1}	Macrostructure	Lap width, mm	Failure load, kN
Load control	250	75		2·7	11·9
Plunge depth control	200	50	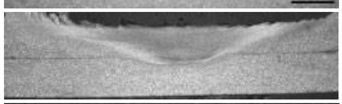	4·5	14·5
	250	75		4·5	14·4

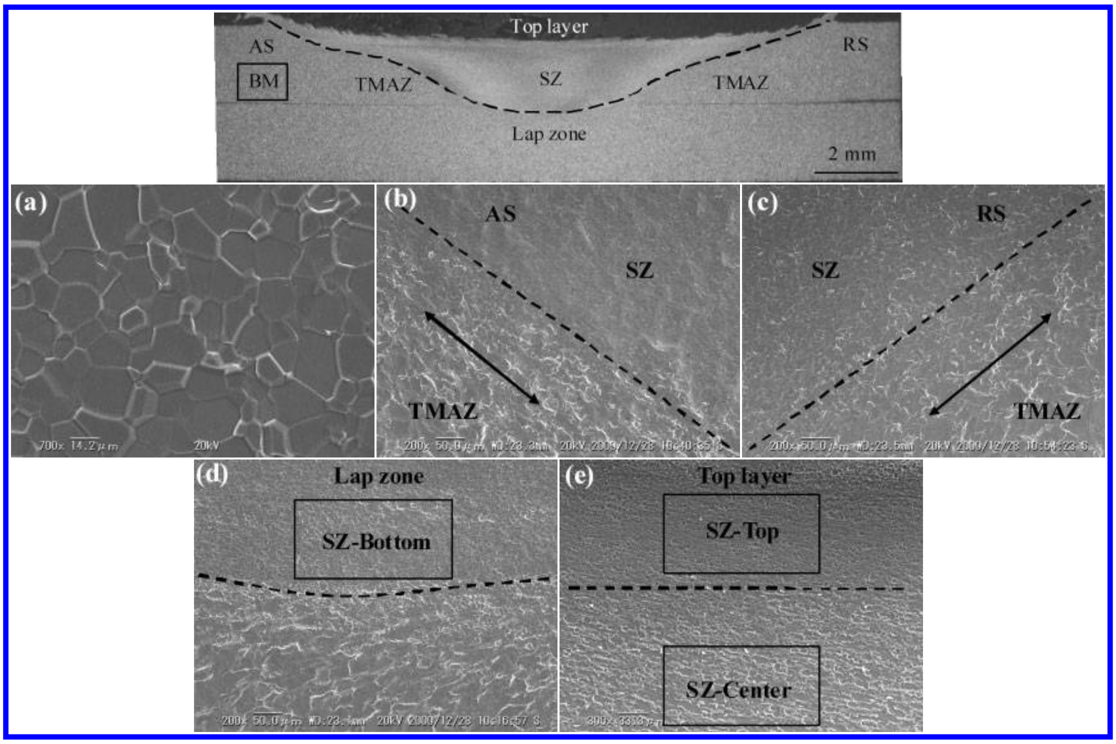

a BM; *b*, *c* TMAZ and SZ; *d* lap zone; *e* top layer

4 Microstructures of sound joint welded at 250 rev min^{-1}–75 mm min^{-1} under tool plunge depth control

with the average size of 6·0 μm (Fig. 5*c*). The bottom part of SZ underwent the lower peak temperature than the centre part during FSW, so the microstructure probably presented the finer grain structure after dynamic recrystallisation. Moreover, as shown in Fig. 5*d*, the top layer indicated the finest grains with an average size of 4·0 μm. The complicated metal flow happened in the region. The metal was stirred by the tool first and then it suffered the reworking with large deformation from the caudal part of shoulder, which possibly caused the further refinement of grain structure.

Conclusions

The groove-like defect formed at low heat input, and the groove-like defect disappeared and the inner cavity defect appeared gradually with increasing heat input. The tool rapidly penetrated into the bottom titanium

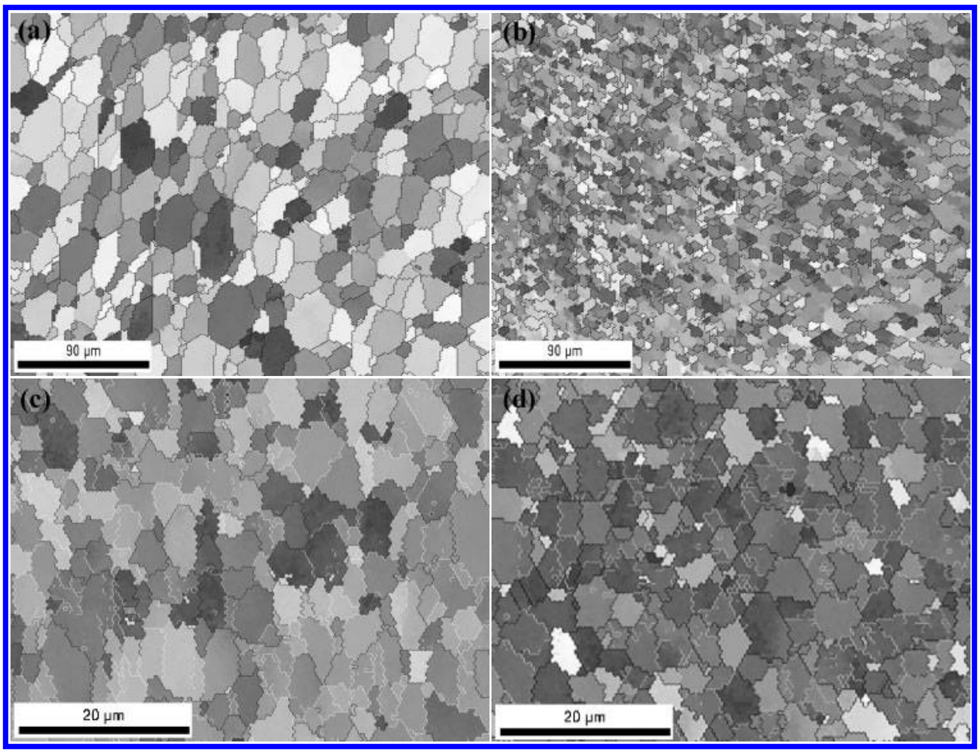

a BM; *b* SZ-Centre; *c* SZ-Bottom; *d* SZ-Top

5 Electron back scattered diffraction maps of different observed regions denoted in Fig. 4

plate under the condition of tool load control when the high heat input was employed, and the overheating rough surface and tool penetration defect was found. The tool plunge depth control effectively increased the lap width compared with the tool load control, so the sound joints fractured in the BM were obtained at 250 rev min^{-1}–75 mm min^{-1} and 200 rev min^{-1}–50 mm min^{-1}. The lap joint was composed of the TMAZ, SZ, the lap zone and the top layer. After welding, the microstructures of the TMAZ and SZ were obviously different from that of the BM. The grain structure with definite deformation direction was found in the TMAZ, and the fine equiaxed grain structure formed in the SZ. The finer grains were detected in the lap zone and top layer, which respectively result from the occurrence of low peak temperature and the reworking from the caudal part of shoulder.

Acknowledgements

The authors give the acknowledgement to Professor H. Fujii for the helpful discussions. They are also grateful to assistant professor T. Tsumura and Dr Y. C. Chen for the kindly technical assistance and useful advice.

References

1. W. M. Thomas, E. D. Nicholas, J. C. Needham, M. G. Murch, P. Templesmith and C. J. Dawes: International Patent Application No. PCT/GB92/02203, 1991.
2. R. S. Mishra and Z. Y. Ma: ‘Friction stir welding and processing’, *Mater. Sci. Eng. R*, 2005, **R50**, 1–78.
3. C. J. Dawes and W. M. Thomas: ‘Friction stir process welds aluminum alloys. The process produces low-distortion, high-quality, low-cost welds on aluminum’, *Weld. J.*, 1996, **75**, 41–45.
4. M. A. Sutton, B. Yang, A. P. Reynolds and R. Taylor: ‘Microstructural studies of friction stir welds in 2024-T3 aluminum’, *Mater. Sci. Eng. A*, 2002, **A323**, 160–166.
5. Y. G. Kim, H. Fujii, T. Tsumura, T. Komazaki and K. Nakata: ‘Three defect types in friction stir welding of aluminum die casting alloy’, *Mater. Sci. Eng. A*, 2006, **A415**, 250–254.
6. Kh. A. A. Hassan, A. F. Norman, D. A. Price and P. B. Prangnell: ‘Stability of nugget zone grain structures in high strength Al-alloy friction stir welds during solution treatment’, *Acta Mater.*, 2003, **51**, 1923–1936.
7. P. Upadhyay and A. P. Reynolds: ‘Effects of thermal boundary conditions in friction stir welded AA7050-T7 sheets’, *Mater. Sci. Eng. A*, 2010, **A527**, 1537–1543.
8. R. Brown, W. Tang and A. P. Reynolds: ‘Multi-pass friction stir welding in alloy 7050-T7451: effects on weld response variables and on weld properties’, *Mater. Sci. Eng. A*, 2009, **A513–A514**, 115–121.
9. S. H. C. Park, Y. S. Sato and H. Kokawa: ‘Effect of micro-texture on fracture location in friction stir weld of Mg alloy AZ61 during tensile test’, *Scr. Mater.*, 2003, **49**, 161–166.
10. L. Yu, K. Nakata and J. Liao: ‘Microstructural modification and mechanical property improvement in friction stir zone of thixo-molded AE42 Mg alloy’, *J. Alloys Compd*, 2009, **480**, 340–346.
11. D. Bakavos and P. B. Prangnell: ‘Effect of reduced or zero pin length and anvil insulation on friction stir spot welding thin gauge 6111 automotive sheet’, *Sci. Technol. Weld. Join.*, 2009, **14**, 443–456.
12. H. K. D. H. Bhadeshia and T. Debroy: ‘Critical assessment: friction stir welding of steels’, *Sci. Technol. Weld. Join.*, 2009, **14**, 193–196.
13. A. P. Reynolds, W. Tang, T. Gnaupel-Herold and H. Prask: ‘Structure, properties, and residual stress of 304L stainless steel friction stir welds’, *Scr. Mater.*, 2003, **48**, 1289–1294.
14. W. M. Thomas, P. L. Threadgill and E. D. Nicholas: ‘Feasibility of friction stir welding steel’, *Sci. Technol. Weld. Join.*, 1999, **4**, 365–372.
15. A. P. Reynolds, W. Tang, M. Posada and J. DeLoach: ‘Friction stir welding of DH36 steel’, *Sci. Technol. Weld. Join.*, 2003, **8**, 455–461.
16. R. Nandan, G. G. Roy, T. J. Lienert and T. Debroy: ‘Numerical modelling of 3D plastic flow and heat transfer during friction stir welding of stainless steel’, *Sci. Technol. Weld. Join.*, 2006, **11**, 526–537.
17. A. J. Ramirez and M. C. Juhas: ‘Microstructural evolution in Ti–6Al–4V friction stir welds’, *Mater. Sci. Forum*, 2003, **426–432**, 2999–3004.
18. W. B. Lee, C. Y. Lee, W. S. Chang, Y. M. Yeon and S. B. Jung: ‘Microstructural investigation of friction stir welded pure titanium’, *Mater. Lett.*, 2005, **59**, 3315–3318.
19. L. Zhou, H. J. Liu, P. Liu and Q. W. Liu: ‘The stir zone microstructure and its formation mechanism in Ti–6Al–4V friction stir welds’, *Scr. Mater.*, 2009, **61**, 596–599.
20. P. Edwards and M. Ramulu: ‘Effect of process conditions on superplastic forming behaviour in Ti–6Al–4V friction stir welds’, *Sci. Technol. Weld. Join.*, 2009, **14**, 669–680.
21. Y. Zhang, Y. S. Sato, H. Kokawa, S. H. C. Park and S. Hirano: ‘Stir zone microstructure of commercial purity titanium friction stir welded using pcBN tool’, *Mater. Sci. Eng. A*, 2008, **A488**, 25–30.
22. S. Mironov, Y. Zhang, Y. S. Sato and H. Kokawa: ‘Crystallography of transformed β microstructure in friction stir welded Ti–6Al–4V alloy’, *Scr. Mater.*, 2008, **59**, 511–514.
23. A. P. Reynolds, E. Hood and W. Tang: ‘Texture in friction stir welds of Timetal 21S’, *Scr. Mater.*, 2005, **52**, 491–494.
24. S. Mironov, Y. S. Sato and H. Kokawa: ‘Development of grain structure during friction stir welding of pure titanium’, *Acta Mater.*, 2009, **57**, 4519–4528.
25. H. Fujii, H. Kato, K. Nakata and K. Nogi: ‘Mechanical properties of friction-stir welded titanium joint’, *Ceram. Trans.*, 2007, **198**, 51–56.
26. K. Reshad Seighalani, M. K. Besharati Givi, A. M. Nasiri and P. Bahemmat: ‘Investigations on the effects of the tool material, geometry, and tilt angle on friction stir welding of pure titanium’, *J. Mater. Eng. Perform.*, 2009, **18**, 1–8.
27. H. Fujii, Y. Sun, H. Kato and K. Nakata: ‘Investigation of welding parameter dependent microstructure and mechanical properties in friction stir welded pure Ti joints’, *Mater. Sci. Eng. A*, 2010, **A527**, 3386–3391.